Predicting Unsteady Pollutant Removal in Green Stormwater Infrastructure with Transit Time Distribution Theory

E. A. Parker[1], S. B. Grant[1,2*], Y. Cao[3,4], M. A. Rippy[1,2], K. J. McGuire[5], P. A. Holden[6], M. Feraud[6], S. Avasarala[7], H. Liu[8], W. C. Hung[9], M. Rugh[9], J. Jay[9], J. Peng[10], S. Shao[11], D. Li[6]

[1]Occoquan Watershed Monitoring Laboratory, Department of Civil and Environmental Engineering, Virginia Tech, 9408 Prince William Street, Manassas VA 20110, USA

[2]Center for Coastal Studies, Virginia Tech, 1068A Derring Hall (0420), Blacksburg, VA 24061, USA

[3]Source Molecular Corporation, 15280 NW 79th Court, St 107, Miami Lakes FL 33016.

[4]Santa Ana Water Quality Control Board, 3737 Main Street, St 500, Riverside CA 92501.

[5]Virginia Water Resources Research Center and Department of Forest Resources and Environmental Conservation, Virginia Tech, Cheatham Hall, 210B, 310 West Campus Drive, Blacksburg, VA 24061

[6]Bren School of Environmental Science and Management, 3508 Bren Hall, UC Santa Barbara, Santa Barbara CA 93106

[7]Department of Earth and Planetary Sciences, University of Tennessee, Knoxville TN 37916 USA

[8]Department of Chemical and Environmental Engineering, Bourns Hall A239, UC Riverside, Riverside, CA 92521

[9]Department of Civil and Environmental Engineering, 420 Westwood Plaza, 5731 Boelter Hall, UCLA Los Angeles, 90095

[10]Orange County Environmental Resources, 2301 Glassell Street, Orange, CA 92865

[11]GSI Environmental Inc., 19200 Von Karman Ave, St 800, Irvine, CA 92612

*Corresponding author: Stanley B. Grant (stanleyg@vt.edu)

Key Points:

- A solution is derived from transit time distribution theory to model the removal of stormwater pollutants in green stormwater infrastructure
- The solution is calibrated and validated with data from 17 simulated storm events at a field-scale test facility in Southern California
- The solution reproduces measured breakthrough concentrations, provided that lateral exchange with the surrounding soil is taken into account

Abstract

In this paper, we explore the use of unsteady transit time distribution (TTD) theory to model pollutant removal in biofilters, a popular form of nature-based or “green” stormwater infrastructure (GSI). TTD theory elegantly addresses many unresolved challenges associated with predicting pollutant fate and transport in these systems, including unsteadiness in the water balance (time-varying inflows, outflows, and storage), unsteadiness in pollutant loading, time-dependent reactions and scale-up to GSI networks and urban catchments. From a solution to the unsteady age conservation equation under uniform sampling, we derive an explicit expression for solute breakthrough with or without first-order decay. The solution is calibrated and validated with breakthrough data from 17 simulated storm events (+/- bromide as a conservative tracer) at a field-scale biofilter test facility in Southern California. TTD theory closely reproduces bromide breakthrough concentrations, provided that lateral exchange with the surrounding soil is accounted for. At any given time, according to theory, more than half of water in storage is from the most recent storm, while the rest is a mixture of penultimate and earlier storms. Thus, key management endpoints, such as the treatment credit attributable to GSI, are inexorably linked to the age distribution of water stored and released by these systems.

Plain Language Summary

Conventional drainage systems are designed to move stormwater as quickly as possible away from cities. By contrast, green stormwater infrastructure (GSI) captures and retains stormwater as close as possible to where the rain falls. As stormwater runoff is a leading cause of non-point source pollution, quantifying the pollutant removal services provided by GSI is a top priority. In this paper we propose and test a mathematical framework—transit time distribution (TTD) theory—for modeling and predicting pollutant removal in biofilters, a popular form of GSI. From field data collected at a biofilter test facility in Southern California, we demonstrate that TTD theory properly accounts for the extreme temporal variability associated with pollutant loading during storms, and the transient unsaturated flow fields that control pollutant fate and transport through the porous media component of these systems. The theory's parsimony and predictive power make it ideally suited to model pollutant removal at the scale of individual biofilters, as well as GSI networks and the urban catchments in which they are embedded.

1. Introduction

Green stormwater infrastructure (GSI) provides many benefits beyond the retention and detention of urban stormwater flows (Walsh et al., 2005; Walsh et al., 2012), including improved water quality, urban heat mitigation, habitat creation resulting in enhanced urban biodiversity, carbon sequestration, recreational opportunities, and mental health (Keeler et al., 2019; Engemann et al., 2019; Raymond et al., 2017; BenDor et al., 2018; Walsh et al., 2016; Grebel et al., 2013; National Academy of Sciences, 2016). In this paper we focus on the water quality benefits of an increasingly popular form of GSI called biofilters, also known as bioretention systems or rain gardens. As illustrated in Figure 1a, these vertically oriented systems filter water through planted soil or sand-based media and are easily integrated into the urban landscape over a range of scales (Roy-Poirier et al., 2010; Wong, 2006). Their possible elements include: (1) a ponding zone that retains water prior to infiltration; (2) biological components including upright vegetation and naturally colonizing soil invertebrates and microorganisms; (3) engineered filter media (sand, sandy loam, or loamy sand with or without media amendments (e.g., biochar; Boehm et al., 2020; Mohanty & Boehm, 2014)); (4) a coarse sand transition layer; (5) a drainage layer consisting of coarse sand or fine gravel which can be lined or unlined and with or without an underdrain; (6) an overflow structure that releases excess stormwater; and (7) a raised outlet to facilitate the formation of a permanently wet “submerged zone” (Kim et al., 2003; Payne et al., 2015; Clar et al., 2004; Rippy, 2015; Grant et al., 2013; Davis et al, 2009).

The water quality benefits attributable to GSI are often quantified based on the fraction of stormwater pollutants (measured on a concentration or mass basis) removed during laboratory or field challenge experiments (Davis et al., 2009; Hatt et al., 2009; Li et al., 2012; Feng et al., 2012; Ulrich et al., 2017; Li & Davis, 2014; Bedan & Clausen, 2009; Kranner et al. 2019). Much of this research has focused on the link between system design and pollutant removal, for example how the choice of plant species and the presence or absence of a submerged zone influences the removal of nutrients (e.g., Kim et al., 2003; Read et al., 2008; Read et al., 2009; Rycewicz-Borecki et al., 2017; Payne et al. 2018) and how media amendments influence the removal of microbial contaminants and heavy metals (e.g., Zhang et al., 2010; Mohanty & Boehm, 2014; Li et al., 2016). The effects of transient unsaturated flow, a defining feature of biofilters and GSI generally, are less often considered. Occasionally, transient unsaturated flow is indirectly acknowledged through experimental designs that incorporate an antecedent dry period between stormwater dosing (Payne et al. 2014; Chandrasena et al. 2014a). Similarly, biofilter design guidelines often recommend the inclusion of a submerged zone so that a portion of stormwater passing through the biofilter spends a longer time undergoing treatment (e.g., nitrogen removal by denitrification) between storms (Payne et al. 2015; LeFevre et al., 2015). Yet, a detailed understanding of how transient unsaturated flow influences contaminant removal remains elusive.

Part of the problem is that transient unsaturated flow imposes severe challenges for predictive modeling. The Richards equation, which describes transient unsaturated flow through porous media, can be solved to estimate time varying flow and saturation through biofilters in one-, two-, or three-dimensions (e.g., using the numerical package Hydrus (Simunek et al., 2008)). These solutions can be coupled to the advection-dispersion equation (ADE) and one or more hypothesized pollutant removal mechanisms, to estimate pollutant removal in biofilters and analogous vadose zone systems (Massoudieh et al., 2017; Radcliffe & Simunek, 2010; Simunek et al., 2008). While this approach may work well as a theoretical exercise (Alikhani, et al., 2020; dos Santos et al., 2013) and under highly controlled conditions in the laboratory (Behroozi et al., 2020; Henrichs et al., 2009; Trenouth & Gharabaghi, 2015; Al-Mashaqbeh & McLaughlan, 2012; Horel et al., 2015) or field (Boivin et al., 2006; Jiang et al., 2010; Massoudieh et al., 2017), its general application is limited by the information required (boundary conditions, soil hydraulic properties, root profiles, and so on) and the fact that biofilters, like the catchments they are nested within, are "complex, heterogeneous, and poorly characterized by direct measurement" (Kirchner, 2009).

Alternatively, mass balance over a control volume drawn around the biofilter media—so-called "bucket models"—can be used to track the temporal evolution of soil moisture and solutes. Daly et al. (2012) used a bucket model to derive the probability density of water volume stored in a biofilter based on a stochastic description of rainfall together with biophysical models for gravitational drainage and evapotranspiration (ET). The power of bucket models lies in their simplicity; an enduring challenge has been how to leverage their output into estimates of pollutant removal. Daly et al. (2012) bridged this gap by relating the pore fluid total nitrogen concentration in a biofilter to soil saturation (estimated from the bucket model) on the premise that low saturation levels are associated with "a reduction in nitrogen plant uptake and denitrification with a consequent accumulation of nitrogen in the filter media that is then washed out during the next inflow event." While clever, this approach does not address the more general problem of predicting pollutant removal as stormwater passes through a biofilter or other GSI.

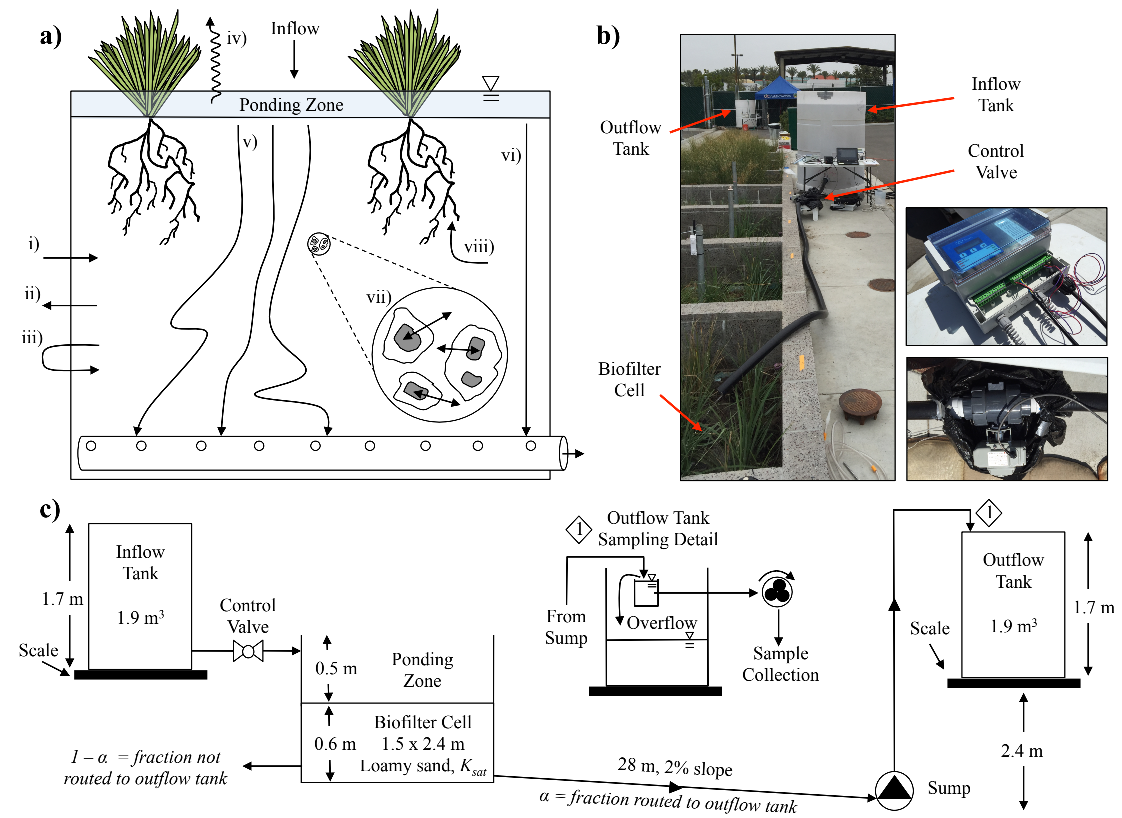

Figure 1. (**a**) Schematic diagram of transport processes that may influence solute transport through the lined biofilter used in our field experiments, including lateral infiltration and exfiltration with the surrounding soil ((i), (ii) and (iii)); outflow by evapotranspiration, gravitational drainage through the filter media, and short-circuiting ((iv), (v), (vi)); diffusive exchange of water and solutes between pore spaces and micro-porosity within individual grains or organic material (vii), and uptake of water and solutes by plant roots (viii). (**b**) Photographs of the experimental set-up at the OCPW Low Impact Development Demonstration Facility (left), and the programmable controller and valve (top and bottom right). (**c**) Detail of the storm simulation experiments, including the vertical and horizontal positions of inflow and outflow tanks, control valve, biofilter test cell, and sampling set-up in the outflow tank (not to scale).

Further, Daly et al.'s bucket model was implemented at a daily time step, and consequently within-storm processes (such as pollutant breakthrough curves) cannot be resolved. Randelovic et al. (2016) proposed a hybrid approach in which the unsteady water balance is solved with a bucket model while pollutant removal in the filter media and submerged zone is predicted with the one-dimensional ADE coupled with one or more pollutant removal mechanisms. Their framework accurately predicts micropollutant removal in field-scale stormwater biofilters (Randelovic et al., 2016) but at the cost of significant complexity—the model consists of 25 coupled equations and requires the specification of 32 variables. Refinements of this model continue to be published (Shen et al., 2018; Zhang et al., 2019) and incorporated into practice oriented GSI design software (e.g., MUSIC (eWater Ltd., 2020)) (reviewed in Jefferson et al., 2017 and Li et al., 2017).

In this paper we propose and test an entirely new approach for predicting unsteady reactive solute transport through GSI: time-variable transit time distribution (TTD) theory. TTD theory combines the simplicity of bucket models with the temporal resolution and physical insights provided by process-based models of pollutant fate and transport in transient unsaturated flow systems. The theory was developed by hydrologists to characterize the myriad transport pathways and timescales associated with water and solute transport through catchments to streams (Rinaldo et al., 2015; Rinaldo et al. 2011) but has since been applied to a diverse array of environmental problems (e.g., Smith et al., 2018; Metzler et al., 2018). In place of a mass conservation equation (such as the ADE), transient TTD theory is premised on a conservation equation for the age distribution of water entering, stored in, and leaving a system. The age distribution of water leaving a system, in turn, encodes all of the information needed to estimate pollutant breakthrough concentrations, including the time history of inflows (e.g., in the case of a biofilter, the magnitude and timing of storm events) and the transformation reactions that occur as water flows through the system along diverse flow paths. In short, TTD theory directly links hydrologic processes to water quality outcomes (Hrachowitz et al., 2016).

There are at least two reasons why TTD theory is a potentially important advance over current approaches for modeling pollutant removal in GSI: (1) *parsimony*; and (2) *extensibility*. The TTD model presented later requires the specification of just one unknown parameter, the effective size of the biofilter (taking lateral exchange of water and solutes with the surrounding soil into account). TTD models can be linked in series and parallel (Bertuzzo et al., 2013; Hrachowitz et al., 2016) to represent GSI networks and the hydrological response units (e.g., hillslopes, groundwater, wetlands, rivers) associated with the urban catchments in which they are embedded. Thus, TTD theory directly addresses a significant limitation with existing GSI modeling frameworks; namely, their "uncertainty in simulating the propagation of flows through pathways such as stormwater networks, pervious runoff and subsurface flows" (Li et al., 2017).

The paper is organized as follows. We begin by developing the TTD modeling framework needed for GSI applications (Section 2). A field-scale test of the TTD theory is then described (Section 3) followed by experimental and modeling results (Section 4), a discussion of water quality implications (Section 5), and conclusions (Section 6).

2. Modeling Framework

The application of TTD theory to GSI entails three steps: (1) a control volume is drawn around the feature of interest, in our case the media of a biofilter; (2) an unsteady water balance is performed over the control volume, taking into account time-varying inflows, outflows, and change in water storage; and (3) the age distribution of water in the control volume, and in water flowing out of the control volume by gravitational drainage and ET, is estimated from TTD theory, along with any water quality metrics (e.g., solute breakthrough curves) of interest. In this section we describe two different approaches for preparing the unsteady water balance, including a simple bucket model (Section 2.1) and the Richards Equation coupled with soil hydraulic functions (Section 2.2). We then solve the age conservation equation (Section 2.3.3) and derive a set of expressions for the age distribution's central tendency and spread (Section 2.3.4) and the breakthrough concentration of a solute with or without first-order decay (Section 2.3.5).

2.1 Bucket Model Water Balance

Equation (1a) is an unsteady macroscopic water balance over the biofilter media, where the variable t [T] is time and the functions $S(t)$ [L], $J(t)$ [L T^{-1}], $Q(t)$ [L T^{-1}], and $\mathrm{ET}(t)$ [L T^{-1}] represent, respectively, the volume of water in storage, infiltration rate of water into the biofilter from the ponding zone, gravitational discharge of water out of the biofilter, and ET across the top boundary of the biofilter (Daly et al., 2012). All volumes and fluxes are normalized by the biofilter's surface area.

$$\frac{dS}{dt}=J(t)-Q(t)-\mathrm{ET}(t) \tag{1a}$$

$$S(t=0)=S_0 \tag{1b}$$

The initial condition (equation (1b)) stipulates that the area-normalized water in storage at time $t=0$ is $S=S_0$ [L]. To solve equation (1a) we must first specify the storage dependence of all terms on the righthand side. These are discussed in turn.

2.1.1 Dependence of Infiltration on Storage

For the field experiments described later, the biofilter is lined and outfitted with an underdrain open to the atmosphere. Under these conditions, a parsimonious description of the infiltration rate can be written as follows, where the variables represent the inflow of stormwater from the surrounding catchment into the ponding zone, $I(t)$ [L T^{-1}], the biofilter media's average saturated hydraulic conductivity, K_{sat} [L T^{-1}], and its maximum water storage volume, $S_{\max}$ [L] (equal to the biofilter's area-normalized void volume):

$$J(t)=\begin{cases} I(t),\ 0<S(t)<S_{\max} \\ K_{sat},\ S(t)=S_{\max} \end{cases} \tag{2}$$

This simple expression approximates the three phases of infiltration (Williams et al., 1998) as follows. Infiltration equals inflow during the *Filling Phase*, which begins when stormwater first enters the ponding zone and infiltration is dominated by capillary forces: $S(t)<S_{\max}$, $J(t)=I(t)$. Infiltration equals the saturated hydraulic conductivity during the *Transition Phase* as the biofilter approaches full saturation: $S(t)=S_{\max}$, $J(t)=K_{\text{sat}}$. During this phase, water level in the ponding zone rises whenever inflow exceeds the media's saturated hydraulic conductivity. Infiltration is zero during the *Draining Phase*, which commences once inflow has ceased and the ponding zone has drained: $S(t)<S_{\max}$, $J(t)=I(t)=0$. While process-based models of infiltration are available (e.g., Green & Ampt, 1911), equation (2) is consistent with the field observations described later (see Section 4) and its sole variables (K_{sat} and $S_{\max}$) are easily measured biofilter design parameters (Payne et al., 2015; Peng et al., 2016; Le Coustumer et al., 2012; Le Coustumer et al., 2009).

2.1.2 Dependence of Gravitational Discharge on Storage

Kirchner (2009) posited that streamflow out of a catchment can be represented by a single non-linear function of the catchment's water storage, $Q(t)=f(S(t))$. One such functional relationship derives from the power-law recessional model for streamflow where the prefactor, a, and exponent, b, are empirical constants:

$$\frac{dQ}{dt} = -a Q^b \tag{3a}$$

When coupled with an unsteady water balance over the catchment, Kirchner demonstrated that equation (3a) can be manipulated to yield an algebraic expression for streamflow as a function of storage (equation (14) in Kirchner (2009)). Here we adopt a rearranged form of Kirchner's algebraic relationship to describe gravitational discharge from a biofilter (equation 3b), where the new variable, S_{min} [L], is the residual storage at which all discharge ceases:

$$Q = K_{\text{sat}} \left(\frac{S - S_{\text{min}}}{S_{\text{max}}} \right)^g \tag{3b}$$

The constants appearing in equations (3a) and (3b) are related as follows:

$$a = g K_{\text{sat}}^{1/g} / S_{\text{max}} \tag{3c}$$

$$b = 2 - 1/g \tag{3d}$$

The new variables, S_{min} and g, are emergent properties of the transient unsaturated flow field; i.e., they must be determined empirically based on experimental observations or numerical solutions of the Richards equation.

2.1.3 Dependence of Evapotranspiration (ET) on Storage

ET also depends non-linearly on water storage, but only when storage falls below a critical value known as the incipient water stress (Allen et al., 1998; Daly et al., 2012). Above the incipient water stress, ET approaches a maximum rate (set by local environmental conditions, including wind speed, vapor pressure deficit, temperature, and plant-specific characteristics) called potential evapotranspiration. While biofilters often operate at or below the incipient water stress (Hess et al., 2019) this was not the case for the experiments described later, which involved simulating a sequence of back-to-back storms. Accordingly, for those experiments we approximated ET with an hourly time series of reference crop potential evapotranspiration (cPET) following FAO guidelines (Allen et al., 1998) and based on measurements at, or nearby, the field site together with plant-specific traits (details in Text S1, Supporting Information (SI)).

2.1.4 Numerical Implementation

The water balance bucket model was solved by substituting into equation (1a) the above expressions for infiltration (equation (2)) and gravitational discharge (equation (3b)), along with hourly estimates of cPET (Section 2.1.3). The model was then forced with timeseries (sampling frequency ~1 min^{-1}) of measured stormwater inflow (Section 3) and numerically integrated following the procedure described in Text S2 (SI). These simulations yielded ~1 min^{-1} timeseries of infiltration, storage and gravitational discharge over the 17 simulated storm events described in Section 3.

2.2 Numerical Solution of the Richards Equation

To calibrate the gravitational discharge term (Section 2.1.2) and as a check on the bucket model predictions described above, ~1 h^{-1} time series of infiltration, storage and gravitational discharge were also simulated with the one-dimensional Richards equation (Hydrus 1D, Version 4.17.0140, PC-Progress, Prague, Czech Republic). The model was forced with measured inflow rates (Section 3) and hourly estimates of cPET (Section 2.1.3). Gravitational discharge from the biofilter's underdrain was represented by a free drainage bottom boundary condition (Jiang et al., 2019). The depth, porosity, and maximum storage of the biofilter were taken as, respectively, $d_b = 0.6$ m, $\theta_s = 0.41$, and $S_{\max} = d_b \theta_s = 0.246$ m (estimated from six cores of the biofilter media collected postexperiment with a 7.6 cm-diameter carbon steel corer). With one exception, we adopted Hydrus 1D's default hydraulic soil parameters for loamy sand (van Genuchten shape parameters $\alpha_{\mathrm{vg}} =$ 12.4 m^{-1} and $n_{\mathrm{vg}} =$ 2.28 [-], residual soil water content $\theta_r =$ 0.057 [-], tortuosity parameter $l = 0.5$ [-]). The exception was saturated hydraulic conductivity, K_{sat}, which was estimated from measurements of peak discharge and in situ measurements with a modified Philip-Dunne Infiltrometer (Text S3, SI).

2.3 Transit Time Distribution (TTD) Theory

2.3.1 Solving the Age Conservation Equation

The age distribution of water in the control volume surrounding the biofilter media is governed by the following age conservation equation (Botter et al., 2011; Harman, 2015):

$$\frac{\partial S_T}{\partial t} = J(t) - Q(t)\bar{P}_Q(T,t) - \mathrm{ET}(t)\bar{P}_{\mathrm{ET}}(T,t) - \frac{\partial S_T}{\partial T} \tag{4a}$$

$$S_T(T,t) = S(t)P_{\mathrm{RTD}}(T,t) \tag{4b}$$

$$S_T(T=0,t) = 0 \tag{4c}$$

$$S_T(T,t=0) = S_0 H(T-T_0) \tag{4d}$$

$$H(x) = \begin{cases} 0, & x<0 \\ 1, & x>0 \end{cases} \tag{4e}$$

The conservation equation's dependent variable, age-ranked storage $S_T(T,t)$ [L], represents the area-normalized volume of water stored in the biofilter media control volume at any time t with ages T or younger. Age-ranked storage is defined mathematically as the product of the area-normalized volume of stored water, $S(t)$, and the cumulative distribution function (CDF) for the fraction of stored water with ages less than or equal to

T; i.e., the stored water's residence time distribution (RTD), $P_{\mathrm{RTD}}(T,t)$ (equation (4b)). As the age variable, T, becomes large, the RTD's CDF tends to unity and the age-ranked storage function collapses to the area-normalized volume of water in storage: $S_T(T \to \infty, t) = S(t)$. The boundary condition (equation (4c)) ensures that no water stored in the control volume has an age less than $T=0$. The initial condition (equation (4d)) implies that, at time $t=0$, the volume of "original" water in storage, S_0, has a single age, $T=T_0$, where the Heaviside function is denoted by $H(x)$. As applied to biofilters, equation (4a) equates the change of age-ranked storage of water in the biofilter media (left hand side) to the infiltration of stormwater of age $T=0$ (first term on right hand side); outflow of water by gravitational discharge (second term) and ET (third term) with age distributions $\overleftarrow{P}_Q(T,t)$ and $\overleftarrow{P}_{\mathrm{ET}}(T,t)$, respectively; and aging of water in storage (fourth term).

The two CDFs appearing in the outflow terms, $\overleftarrow{P}_Q(T,t)$ and $\overleftarrow{P}_{\mathrm{ET}}(T,t)$, represent the fraction of water leaving the biofilter as gravitational discharge and ET with ages T or less at time t. The backward arrows on these CDFs indicate they are "backward TTDs"; i.e., they represent the age distribution of water *leaving* the biofilter at time t. A corresponding set of forward TTDs can be written for the "life expectancy" of water parcels entering the biofilter at time, t_i. The relationship between forward and backward TTDs is given by Niemi's Theorem (Niemi, 1977; Benettin et al., 2015a; Harman, 2015). Under unsteady hydrology, the backward TTDs for gravitational discharge and ET are not necessarily equal, nor are they necessarily equal to the RTD of water in storage (Botter et al., 2011).

2.3.2 Ranked StorAgeSelection (rSAS) Function

As written, equation (4a) is mathematically ill posed because it consists of a single equation with three unknown functions: $S_T(T,t)$, $\bar{P}_Q(T,t)$, and $\bar{P}_{\mathrm{ET}}(T,t)$. This closure problem can be resolved by introducing a new CDF, the ranked StorAgeSelection (rSAS) function, $\Omega(S_T,t)$ [-], which maps the fraction of outflow with ages less than or equal to T (i.e., the CDF form of the backward TTD for discharge or ET) to the fraction of age-ranked water in storage with that age or younger "selected" for outflow by either drainage or ET (Botter et al., 2011; Harman, 2015):

$$\bar{P}(T,t)=\Omega\left(S_T(T,t),t\right) \tag{5a}$$

In principle, the functional form of the rSAS function can be calculated by averaging the ADE for solute transport over the control volume (Benettin et al., 2013; Rinaldo et al., 2015). For the purposes of this study, we adopted a "uniform rSAS" function, under the assumption that water in storage has an equal probability of being selected for outflow regardless of its age (Harman, 2015):

$$\Omega_Q(S_T,t)=\Omega_{\mathrm{ET}}(S_T,t)=S_T(T,t)/S(t),\quad S_T(T,t)\in\left[0,S(t)\right] \tag{5b}$$

Uniform rSAS functions often apply to systems, such as ours, that are far from well-mixed (Bertuzzo et al., 2013; Benettin et al., 2013; Benettin et al., 2015b; Kim et al., 2016; Rodriguez et al., 2018; Danesh-Yazdi et al., 2018).

2.3.3 Exact Solution for Age-Ranked Storage under Uniform Selection

Under uniform sampling the age conservation equation (equation 4a) can be solved exactly for certain choices of initial and boundary conditions (Botter et al., 2011; Bertuzzo et al., 2013). Equation (6a) is one such solution that satisfies the initial and boundary conditions presented earlier (equations (4c) and (4d), see Text S4 (SI) for derivation); the superscript "U" denotes uniform storage selection.

$$S_{\mathrm{T}}^{U}\left(T,t\right)=e^{-\bar{f}_{Q}(t)-\bar{f}_{\mathrm{ET}}(t)}\left[S_{0}H\left(T-t-T_{0}\right)+\int_{a}^{t}e^{\bar{f}_{Q}(v)+\bar{f}_{\mathrm{ET}}(v)}J\left(v\right)dv\right] \tag{6a}$$

$$a=\begin{cases}0, & T-t\geq 0\\ t-T, & T-t<0\end{cases} \tag{6b}$$

$$\bar{f}_{Q}\left(v\right)=\int_{0}^{v}\frac{Q\left(u\right)}{S\left(u\right)}du \tag{6c}$$

$$\bar{f}_{\mathrm{ET}}\left(v\right)=\int_{0}^{v}\frac{\mathrm{ET}\left(u\right)}{S\left(u\right)}du \tag{6d}$$

According to equation (6a) age-ranked storage (left hand side) is influenced by the evolving age distribution of both "original" water in storage at time $t=0$ (first term on right hand side) and "young water" that infiltrates during storm events (second term). This solution was numerically integrated (details in Text S4 (SI)) to yield ~1 min^{-1} timeseries of age-ranked storage in the biofilter, after substituting bucket model simulations for infiltration, $J(t)$, storage, $S(t)$, and gravitational discharge, $Q(t)$ (Section 2.1).

2.3.4 Age Structure of Stored Water in the Biofilter

Under uniform selection the backward TTDs for gravitational discharge and ET are equal, and equal to the RTD of water in storage (compare with equation (4b)) (Harman, 2015):

$$P_{\mathrm{RTD}}\left(T,t\right)=\overleftarrow{P}_{Q}\left(T,t\right)=\overleftarrow{P}_{\mathrm{ET}}\left(T,t\right)=\frac{S_{T}\left(T,t\right)}{S\left(t\right)}=\frac{e^{-\bar{f}_{Q}(t)-\bar{f}_{\mathrm{ET}}(t)}}{S\left(t\right)}\left[S_{0}H\left(T-t-T_{0}\right)+\int_{a}^{t}e^{\bar{f}_{Q}(v)+\bar{f}_{\mathrm{ET}}(v)}J\left(v\right)dv\right] \tag{7a}$$

The 5$^{\mathrm{th}}$, 50th, and 95$^{\mathrm{th}}$ percentile ages of water in storage and outflow at any time, t, can be obtained from equation (7a) by numerically solving the following implicit equations for water age: $S_{T}\left(T_{0.05},t\right)/S\left(t\right)=0.05$, $S_{T}\left(T_{0.5},t\right)/S\left(t\right)=0.5$, and $S_{T}\left(T_{0.95},t\right)/S\left(t\right)=0.95$. The age-ranked storage's probability density function (PDF) can be calculated from equation (7a) by differentiation where the symbol δ denotes the Dirac delta function:

$$p_{\mathrm{RTD}}^{U}\left(T,t\right)=\overleftarrow{p}_{Q}^{U}\left(T,t\right)=\overleftarrow{p}_{\mathrm{ET}}^{U}\left(T,t\right)=\frac{\partial P_{\mathrm{RTD}}^{U}}{\partial T}=\delta\left(t+T_{0}-T\right)\frac{S_{0}}{S\left(t\right)}e^{-\overline{f}_{Q}\left(t\right)-\overline{f}_{\mathrm{ET}}\left(t\right)}+H\left(t-T\right)\frac{J\left(t-T\right)}{S\left(t\right)}e^{-\overline{f}_{\mathrm{ET}}\left(t\right)+\overline{f}_{\mathrm{ET}}\left(t-T\right)-\overline{f}_{Q}\left(t\right)+\overline{f}_{Q}\left(t-T\right)}$$

(7b)

The mean age in storage and outflow immediately follows by taking the first moment of the PDF for age-ranked storage:

$$\mu_{\mathrm{RTD}}^{U}\left(t\right)=\mu_{Q}^{U}\left(t\right)=\mu_{\mathrm{ET}}^{U}\left(t\right)=\int_{0}^{\infty}v\,p_{\mathrm{RTD}}^{U}\left(v,t\right)dv=\frac{1}{S\left(t\right)}\left[S_{0}e^{-\overline{f}_{Q}\left(t\right)-\overline{f}_{\mathrm{ET}}\left(t\right)}\left(t+T_{0}\right)+\int_{0}^{t}\left(t-u\right)J\left(u\right)e^{-\overline{f}_{\mathrm{ET}}\left(t\right)+\overline{f}_{\mathrm{ET}}\left(u\right)}e^{-\overline{f}_{Q}\left(t\right)+\overline{f}_{Q}\left(u\right)}du\right]$$

(7c)

Further details on the derivation and numerical implementation of equations (7b) and (7c) are described in Text S5 (SI).

2.3.5 A TTD Theory for Solute Fate and Transport through a Biofilter

The concentration of a reactive or non-reactive (i.e., conservative) solute in water leaving the biofilter by gravitational discharge, $C_{Q}\left(t\right)$, can be calculated by convolving the PDF of the backward TTD (equation (7b)) with the concentration of solute, $C_{J}\left(t_{i},T\right)$, that entered the biofilter at time, $t_{i}=t-T$, and exited the biofilter as gravitational discharge at time t and age T (Harman, 2015):

$$C_{Q}\left(t\right)=\int_{0}^{t}C_{J}\left(t-T,T\right)\overleftarrow{p}_{Q}\left(T,t\right)dT \qquad (8a)$$

Despite its simplicity, this convolution integral incorporates a rich set of processes, including unsteadiness in the biofilter's water balance (e.g., time-varying inflows, outflows, and storage, through the time-evolution of the backward TTD), unsteadiness in the solute concentration entering the biofilter from the ponding zone (through the dependence of $C_{J}\left(t_{i},T\right)$ on the inflow time, $t=t_{i}$) and any time-dependent reactions that occur as a solute passes through the biofilter. For example, if the solute undergoes first-order reaction, the function $C_J(t_i,T)$ takes on the following form where the new variable k [T^{-1}] is a first-order rate constant (Harman, 2015):

$$C_J(t_i,T)=C_J(t_i)e^{-kT} \tag{8b}$$

Combining equations (7b), (8a), and (8b) we arrive at the following solution for the concentration of a reactive solute in water discharged from the biofilter, where C_0 is the concentration of solute present in the original water stored in the biofilter at time, $t=0$:

$$C_Q(t)=C_0\frac{S_0e^{-k(t+T_0)-\bar{f}_Q(t)-\bar{f}_{\mathrm{ET}}(t)}}{S(t)}+\frac{1}{S(t)}\int_0^t C_J(u)J(u)e^{-k(t-u)-\bar{f}_{\mathrm{ET}}(t)+\bar{f}_{\mathrm{ET}}(u)-\bar{f}_Q(t)+\bar{f}_Q(u)}\,du \tag{8c}$$

For the experiments described later, a subset of 17 simulated storms were tagged with bromide, which we assumed behaved conservatively. The inflow concentration for these storms can be expressed as follows, where $C_{J,m}$, $t_{m,s}$, and $t_{m,e}$ are the m-th storm's bromide concentration, start time and end time, respectively, and the sum is taken over all N storms:

$$C_J(t_i)=\sum_{m=1}^{N}C_{J,m}H(t_i-t_{m,s})H(t_{m,e}-t_i) \tag{9a}$$

Substituting equation (9a) into equation (8c), setting $C_0=0$ (because, in our experiments, no bromide was present in the biofilter's original water), setting $k=0$ (because bromide is assumed to be conservative) and using the distributive property of integration, we arrive at the following expression for bromide concentration in water leaving the biofilter by gravitational discharge (details of derivation in Text S6 (SI)):

$$C_Q(t)=\frac{1}{S(t)}\sum_{m=1}^{N}C_{J,m}H(t-t_{m,s})\int_{t_{m,s}}^{b}J(u)e^{-\bar{f}_{\mathrm{ET}}(t)+\bar{f}_{\mathrm{ET}}(u)-\bar{f}_Q(t)+\bar{f}_Q(u)}\,du \tag{9b}$$

$$b = \begin{cases} t, \ t < t_{m,e} \\ t_{m,e}, \ t \geq t_{m,e} \end{cases} \quad (9c)$$

In deriving equation (9b) we have assumed that plants in the biofilter take up bromide and water in the same proportion, which may not be the case in practice (e.g., if a solute is excluded from plant uptake its pore fluid concentration will increase over time by in situ evaporative concentration (Bertuzzo et al., 2013; Harman, 2015)). However, ET represents a very small portion of the the overall water balance for the field experiments described later (Section 4) and hence in situ evaporative concentration can be neglected in our case. Time series (~1 min^{-1}) of bromide breakthrough concentration were simulated with equation (9b) following the numerical procedures described in Text S6 (SI).

3. Field Methods

3.1 Orange County Public Works (OCPW) Biofilter Test Facility

Field-scale biofilter challenge experiments were carried out at the Orange County Public Works (OCPW) low impact development demonstration facility located in the City of Orange, Orange County, California. Experiments were conducted in a biofilter test cell (approximately 2.4 m x 1.5 m x 0.6 m deep) built by a local contractor with previous GSI construction experience (Tobo Construction, Figure 1b). The test cell, which was lined and outfitted with an underdrain, consisted of a concrete slab floor and four cinderblock walls extending approximately 0.5 m above the filter media surface to create a ponding zone (Figures 1b, 1c). The filter media consisted of sand (65%), sandy loam (20%), and compost (15%) (v/v basis). In January 2017, the media was planted with a European grey sedge, *Carex divulsa tumulicola*. When we conducted our first set of experiments in the summer of 2018 the plant community also included opportunist ruderal weed species (e.g., the common dandelion).

The research team retrofitted the biofilter with an upstream 1890 L "inflow" tank (Custom Roto-Molding, Inc., Caldwell, ID) which drained by gravity through a programmable control valve (Sigma Controls, Inc., Perkasie, PA) to the biofilter's ponding zone (Figure 1b). The weight of the inflow tank was monitored continuously at ~10 Hz (WinWedge, TAL Technologies Inc., Philadelphia, PA) with a calibrated industrial scale (PCE-SW 3000N Pallet Scale, PCE Americas Inc., Jupiter, FL). The weight measurements were lowpass filtered (Davis, 2002), differentiated, and divided by the density of water to yield ~1 min^{-1} estimates for the volumetric discharge of water entering the ponding zone, $I(t)$. Following the experiments conducted in the summer of 2018 we discovered that, during construction, a ca., 5 cm diameter hole had been drilled through the base of the cinderblock wall separating our test cell from the adjacent test cell (and through the wall separating the adjacent test cell from the next test cell and so on) to accommodate a buried irrigation pipe. A substantial fraction of stormwater added to our test cell (approximately 50%) laterally exfiltrated to the adjacent cell through this hole. While not part of our original design, this feature made for a more realistic field experiment, as most operational biofilters undergo at least some degree of subsurface exfiltration (e.g., Brown & Hunt, 2011). Indeed, our exfiltration rate of ~50% is close to the stormwater volume reduction design goal for GSI of 67% (Davis, 2008). To model lateral exfiltration, gravitational discharge from the biofilter was routed as follows. A fixed fraction, α, was assigned to the underdrain and the rest, $1-\alpha$, to lateral exfiltration to the adjacent test cell (Figure 1c). The fraction α was estimated using several independent experimental methods (Text S7 and Figure S1, SI).

Water exiting the biofilter through the underdrain flowed by gravity through a buried manifold to an underground sump and from there was periodically pumped (Model 98 Sump Pump, Zoeller Pump Company, Louisville, KY) up to an "outflow" tank sitting on a calibrated industrial scale at ground level (identical to the inflow tank set up, Figure 1c). A timeseries (~1 min^{-1}) of volumetric discharge entering the outflow tank was estimated from high frequency (10 Hz) measurements of the tank's weight following the same procedure described above for the inflow tank. Time series of volumetric discharge and bromide concentration measured at the outflow tank were time-shifted backwards by 30 minutes to account for the transit of water from the biofilter's underdrain to the outflow tank and the overly fast response of the bucket model to storm events (Text S8, SI).

3.2 Experimental Storm Hydrograph

Municipal separate storm sewer system (MS4) permit requirements for the Santa Ana Region (where our experiments were carried out) stipulate that new development and significant re-development projects include stormwater control measures sufficient to capture runoff volume generated by the 85th percentile storm, which at this field site corresponds to 0.84 inches of stormwater depth (volume per unit catchment area) over a 24-hour period (OCPW, 2017). With this regulatory requirement in mind, we designed our experimental storm hydrograph as follows: (1) seven 24-hour rainfall events were selected from measurements at an onsite rain gauge over the time period 2011 to 2016; (2) an average hyetograph was constructed from these seven events after aligning peaks and standardizing the total 24-hour rainfall depth to 0.84 inches; and (3) a design storm hydrograph was calculated from the average hyetograph by the Rational Method (Brooks et al., 2013) assuming a unit runoff coefficient (corresponding to 100% imperviousness) and a catchment area of 82.3 m^2. The corresponding biofilter-to-catchment area ratio (4.5%) is typical for urban landscapes in Southern California (Ambrose & Winfrey, 2015). See Text S9 and Figure S2 (SI) for a comparison of measured and design storm hydrographs.

3.3 Bromide Tracer Experiments

A sequence of storms (each of which conformed to the storm hydrograph described in Section 3.2) were discharged to our experimental biofilter over a five-day period in the summer of 2018 (June 25-29) and again over a five-day period in the summer of 2019 (June 1-5). Ten storms were simulated in 2018, one in the morning and another in the afternoon on each day. The afternoon storms were spiked with bromide (final concentration ~50 Br^- mg/L) while the morning storms were bromide free. The storm sequence in 2019 consisted of: (1) two bromide-free storms on the first day, one in the morning and one in the afternoon; (2) two days later a single bromide-spiked storm in the morning (final concentration of 124 Br^- mg L^{-1}); and (3) over the following two days two bromide-free storms per day, one in the morning and one in the afternoon. Three replicate 40 mL samples were collected from the inflow tank before each simulated storm. Outflow samples were collected as follows. Water entering the outflow tank from the sump was directed into a continuously overflowing 5 L bucket affixed to the top of the tank (the bucket overflowed into the tank, see Figure 1c). Water in the bucket was continuously sub-sampled (40 mL min^{-1}) by means of a peristaltic pump (BioLogic LP, Bio-Rad, Hercules, CA) and fractionated into 50 mL conical tubes (Falcon, Corning Life Sciences, Tewksbury, MA) according to a pre-defined sampling schedule (2018: every 2, 5, or 10 minutes, with more rapid sampling during the first hour of biofilter outflow; 2019: every 5 minutes) (inset, Figure 1c). During each storm, outflow samples were collected in this manner until the on/off cycling of the sump pump fell below 1/30 min^{-1}. The bromide concentration in each sample was measured by ion chromatography (2018: 940 Professional IC Vario, Metrohm AG, Herisau, Switzerland; 2019: Dionex DX-120, Thermo Fisher Scientific, Waltham, MA). A total of N=30 (15) and 435 (147) inflow and outflow samples, respectively, were analyzed during the 2018 (2019) experiments.

In addition to the timing of storm events and the periodic (2018) and non-periodic (2019) nature of the bromide dosing, the 2018 and 2019 experiments differed in several other respects (details in Text S9, SI), including: (1) the nature of the water used (tap water in 2018 and stormwater +/- sewage in 2019); (2) the partial sealing of the hole in the test cell wall after 2018; (3) the method used to reproduce the design storm; and (4) change in plant community from a European grey sedge and ruderal weeds in 2018 to a native southern California sedge in 2019.

4. Results and Discussion

4.1 Lateral Exfiltration and the Effective Volume of the Biofilter

During each experimental storm we discharged roughly the same volume of water (~1400 L) to the biofilter's ponding zone over one to two hours. The volume of water captured in the outflow tank varied by storm, from 378 to 751 L (25 to 49% of the inflow volume) for the ten experiments conducted in 2018, and from 266 to 654 L (21 to 46% of the inflow volume) for the seven experiments conducted in 2019 (Table S1, SI). Across all 17 storms, ET was a minor component of the water budget (< 0.3% of the ~1400 L added per storm,

Table S1, SI). Thus, the difference between these inflow and outflow volumes either went to increasing storage or lateral exfiltration to the adjacent test cell (see Text S7, SI).

The fraction of inflow volume recovered at the outflow tank is inversely correlated with each storm's antecedent dry period (R^2=0.82, Figure S1, SI), consistent with the hypothesis that at least some of the unrecovered water goes to storage. Extrapolating the fractional water recovery back to an antecedent dry period of zero hours (under the premise that the change in storage should be zero in this case) we estimate that, in both 2018 and 2019, approximately $\alpha = 46$% of the water added to the biofilter is routed to the outflow tank while $1-\alpha = 54$% is lost to lateral exfiltration (Text S7, SI). These results are consistent with loss rates measured under steady-state flow conditions (Text S7, SI) and the observed wetting of biofilter media in the adjacent test cell (data not shown), along with previously published modeling studies (Browne et al., 2008; Lee et al., 2015) and field measurements (Winston et al., 2016) that indicate exfiltration is a dominant mechanism for volume reduction in GSI. At our site, some of the exfiltrated water and solute may eventually find its way back to the outflow tank, for example by circulating back through our biofilter test cell (mechanism (iii), Figure 1a) or transiting along another subsurface route to the buried collection manifold (indeed, the test cell adjacent to our biofilter also had an underdrain that could have contributed flow and solute to the manifold and, ultimately, to the outflow tank). Thus, exfiltration can potentially increase the effective volume of our biofilter during solute transport (we return to this idea in Section 4.4).

4.2 Power-Law Model for Gravitational Discharge

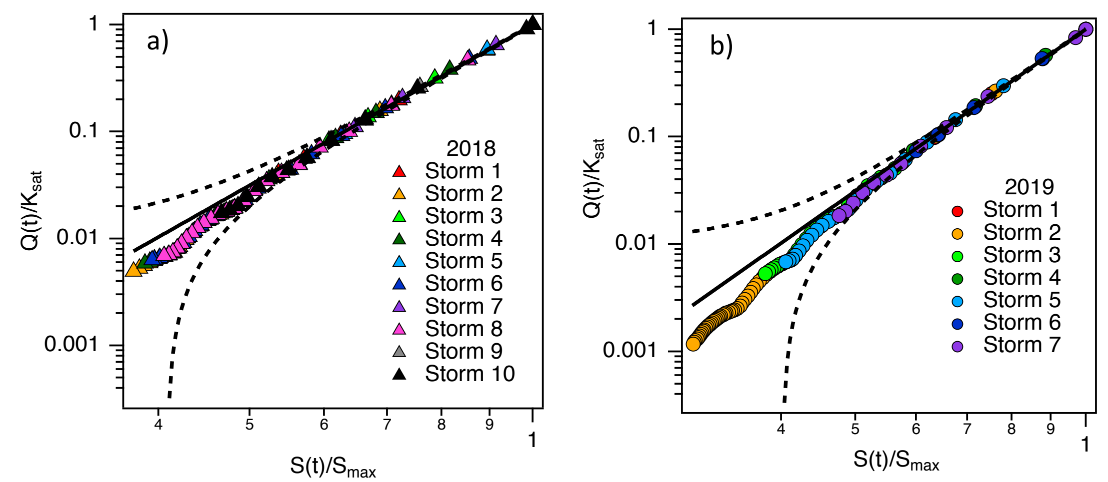

Figure 2. Power-law dependence of gravitational discharge on water storage simulated with Hydrus 1D for storm sequences in (**a**) 2018 and (**b**) 2019. Solid and dashed black curves indicate model fit and 95% prediction intervals, respectively.

Kirchner's power-law model for gravitational discharge (equation 3b) could not be evaluated using our inflow and outflow measurements, because lateral exfiltration from the test cell precluded accurate estimates for the gravitational discharge and water storage terms (Section 4.1). Instead, hourly time series for these two quantities were numerically simulated, with Hydrus 1D, over the seventeen experimental storms in 2018 and 2019 (Section 2.2). Consistent with Kirchner's power-law relationship, when normalized and plotted on a log-log basis, the Hydrus-generated time series of discharge and storage collapse to a single line for $Q(t)>0.05K_{sat}$ (Figure 2). Inferred values of the power-law exponent and minimum storage value are the same, within error, across both years (2018: $g=4.99\pm0.01$ and $S_{min}=-3.6\times10^{-20}\pm1.9\times10^{-4}$; 2019: $g=5.00\pm0.01$ and $S_{min}=-3.4\times10^{-21}\pm2.2\times10^{-4}$). Thus, these two parameters are robust to changes in the sequence and length of antecedent dry periods as well as changes in saturated hydraulic conductivity (within each simulated storm sequence, the saturated hydraulic conductivity declined over time, see Text S3, SI). Our power-law exponent is also concordant with values inferred by

Bertuzzo et al. (2013) for gravitational drainage from the vadose zone of a 46 km^2 catchment in Switzerland (compare $g=5$ with the posterior distribution for the exponent c in their Figure 4). Substituting $g=5$ into equation (3d) yields a recessional exponent of $b=$ 1.8, which is toward the flashy end of the allowable range, $b\in[1,2]$ (Kirchner, 2009), in keeping with the small storage volume of our biofilter (e.g., compared to the volume of water stored in a catchment). In summary, these results support the hypothesis that Kirchner's power-law relationship (equation (3b)) applies at the scale of a single biofilter.

4.3 Unsteady Water Balance: Bucket Model and Hydrus 1D Predictions

Over the 17 experimental storms conducted during 2018 and 2019, numerical solutions of the bucket model (equation (1a)) closely follow Hydrus 1D simulations of ponding depth, biofilter saturation, and gravitational discharge (Figure 3). The predicted range of ponding depths (from 0 to 0.2 m above the surface of the biofilter media) is consistent with field observations and the predicted gravitational discharge rates closely match measurements at the outflow tank (light blue curves, bottom panels of Figures 3a and 3b).

4.4 TTD Theory Predictions for Bromide Transport

To characterize the transport of solute through the experimental biofilter, we spiked a subset of experimental storms with bromide as a conservative tracer. In 2018, we adopted a semi-periodic study design involving, on each day, a bromide-free "flushing" storm in the morning (orange arrows in Figure 4a) and a bromide-spiked "tracer" storm in the afternoon (black arrows in Figure 4a). By the second day of the storm sequence, the normalized bromide breakthrough curves (BTCs) settled into a periodic pattern, oscillating between $C_Q/C_{J,1}\approx$ 0.3 and 0.6 during the morning and afternoon storms, respectively (black dots in lower graph, Figure 4a). Here, the variable $C_Q(t)$ represents the measured

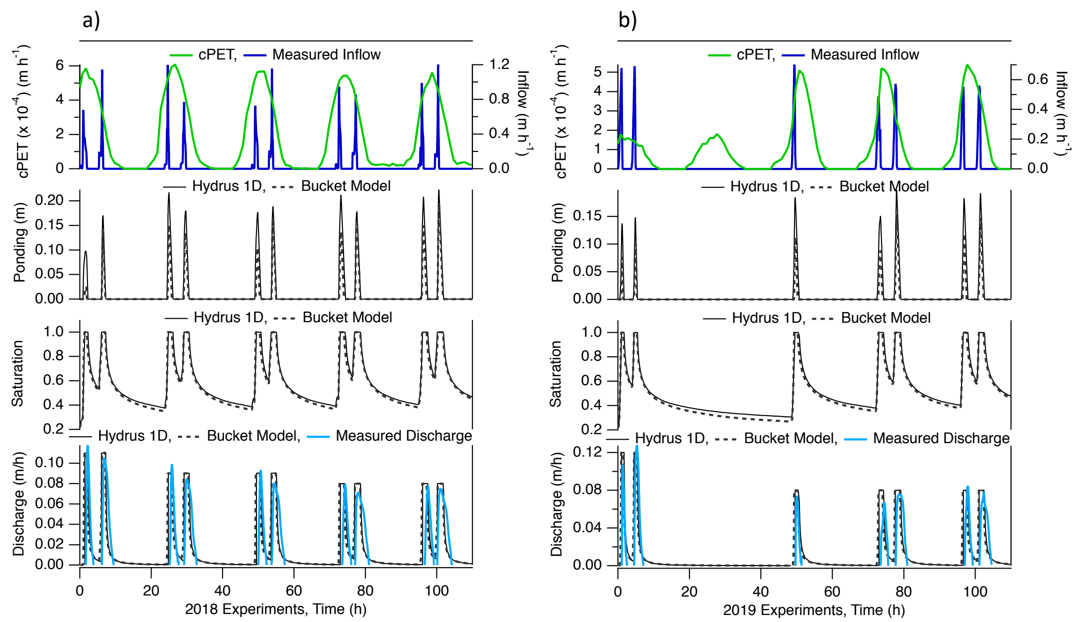

Figure 3. Two approaches for simulating the unsteady water balance in our biofilter: numerical solutions to the Richards equation (Hydrus 1D, solid black curves) and a bucket model (dashed black curves). Colored lines represent measured inflow (dark blue), measured outflow (light blue) and calculated cPET (green) for the set of experiments conducted during the summers of (**a**) 2018 and (**b**) 2019. To compare simulated and measured discharge, the former was multiplied by $\alpha = 0.46$ and the latter was backward time shifted by 30 min.

bromide concentration at the outlet tank and the variable $C_{J,1}$ = 48.7 mg L^{-1} represents the initial bromide concentration measured in the first afternoon tracer storm (across all five tracer storms the initial bromide concentrations were $C_{J,m} = 48.7$, 48.8, 49.3, 48.3, and 44.4 mg L^{-1}). The bromide BTC predicted by TTD theory also follows a periodic pattern (solid curve, bottom graph, Figure 4a), but the model consistently under- and over-predicts measured bromide concentrations in the morning and afternoon storms, respectively. These model predictions were calculated from equation (9b) after specifying the timing and initial bromide concentrations associated with each bromide-spiked storm, and running bucket model simulations for $J(t)$, $S(t)$, and $Q(t)$ after setting the maximum volume equal to the actual void volume of the biofilter, $S_{\max} = 0.246$ m. The TTD model's

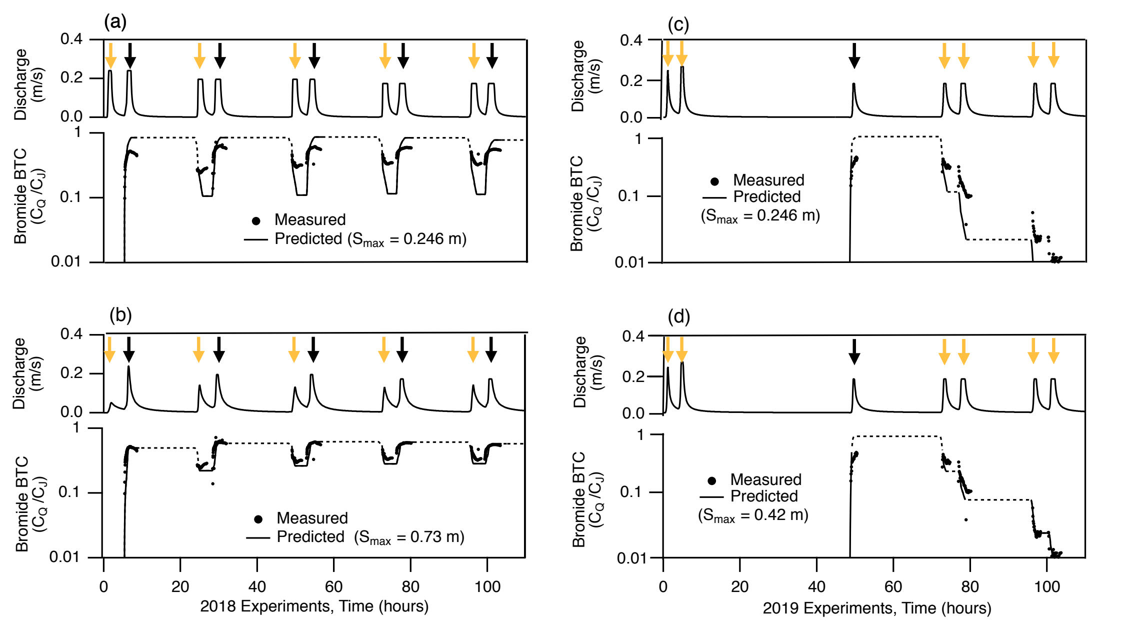

Figure 4. Comparison of measured (points) and predicted (solid and dashed curves) bromide breakthrough curves (BTCs) for the 2018 ((a) and (b)) and 2019 ((c) and (d)) experiments. Model predictions assume S_{max} equals the physical volume of the biofilter ((a) and (c)) or a volume obtained by fitting the model to the second storm of 2018 (b) or the fourth, fifth, sixth, and seventh storms of 2019 (d). Dashed curves correspond to times when no samples were collected. Vertical arrows mark the bromide-spiked (black) and bromide-free (orange) storms. Each panel also includes bucket model predictions for gravitational discharge given the value of S_{max} shown.

tendency to overshoot bromide measurements implies it is oversampling young water; i.e., the predicted bromide BTC contains too much bromide-free water during the bromide-free morning storm, and too much bromide-spiked water during the bromide-spiked afternoon storm.

One possible explanation is that the uniform storage selection function, which underpins our model (see equation (9b) and discussion thereof), oversamples young water for gravitational discharge. Alternatively, the storage selection function is fine but there is not enough old water in storage to select from. While the former explanation cannot be ruled out (indeed, the science of selecting rSAS functions is an active area of current research (Harman, 2019)), the latter explanation is compelling for several reasons. First, the void volume of our biofilter (~900 L) is less than the volume of water flowing into the biofilter with each experimental storm (~1400 L). Therefore, as far as the model is concerned, the biofilter has very limited capacity to store older water from penultimate and older storms. Second, a substantial fraction (>50%) of the inflow volume leaves our biofilter by lateral exfiltration. As noted in Section 4.1, some of this exfiltrated water may eventually return to the outflow tank and thereby increase the effective volume that solutes experience as they transit through the system.

To test the last hypothesis—that the effective volume for solute transport is larger than the biofilter's physical volume—we split the measured bromide data from 2018 into a calibration period (the first bromide-spiked storm, storm #2) and a validation period (all other storms). We then inferred a value of the biofilter's void volume by minimizing the root-mean square error (RMSE) over the calibration period (Figure S3, SI). The optimal volume thus obtained ($S_{\max}=0.73$ m) is about two times larger than the physical volume of the biofilter ($S_{\max}=0.246$ m) consistent with the hypothesis that a substantial fraction of the exfiltrated water eventually returns to the outflow tank. When the inferred value of $S_{\max}=0.73$ m is substituted back into the bucket model and the hydrologic water balance is recomputed, equation (9b) closely tracks the bromide BTC over the validation period (storms #3 through #10, bottom graph in Figure 4b).

Application of TTD theory to the 2019 storm sequence yields similar results. If the maximum volume of the biofilter is set equal to its physical volume ($S_{\max}=0.246$ m), equation (9b) consistently under-predicts bromide breakthrough during the four bromide-free flushing storms (storms #4, 5, 6, and 7, bottom graph in Figure 4c). However, when the effective volume is raised to $S_{\max}=0.42$ m (obtained by minimizing the RMSE for

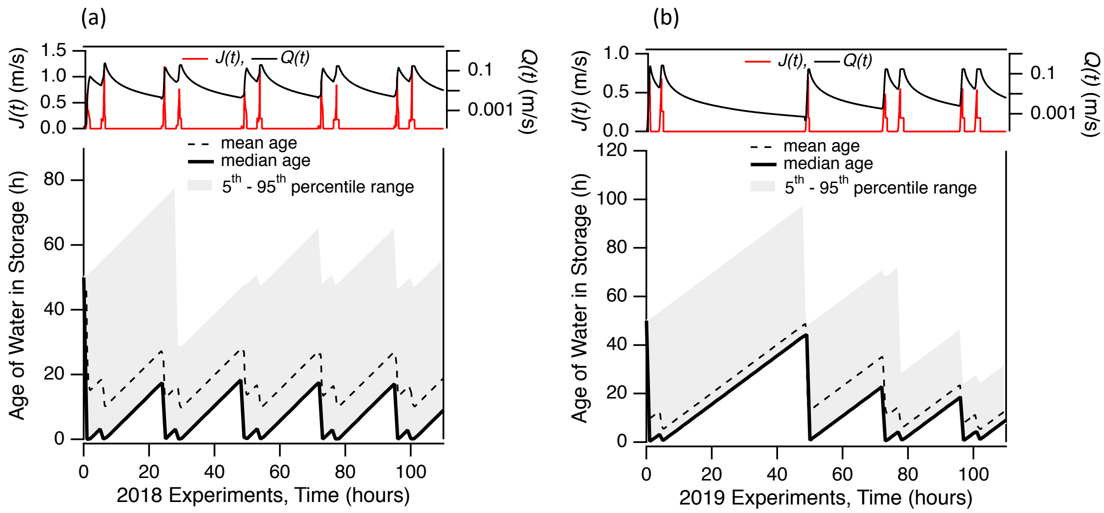

Figure 5. The evolution of mean and median water ages in the biofilter during the sequence of storms in (a) 2018 and (b) 2019. Also shown are the 5th to 95th percentile range (grey band). Top panels indicate the infiltration (red curve) and gravitational discharge (black curve) rate for each storm sequence. For these simulations, we adopted inferred values of maximum storage: $S_{\max} =$ 0.73 and 0.42 m for 2018 and 2019, respectively. The age of water of original water was arbitrarily set to $T_0 = 50$ h and its volume was taken as the product of initial saturation ($s_0 = 0.22$, corresponding to field capacity) and maximum storage: $S_0 = s_0 S_{\max}$.

storms #4 through 7, see Figure S3, SI) the model's performance improves markedly (Figure 4d). The void volume inferred from the 2018 experiments ($S_{\max} = 0.73$ m) is about 74% larger than the void volume inferred from the 2019 experiments ($S_{\max} = 0.42$ m). This difference could reflect biophysical changes in the biofilter test cell over the two years (e.g., after the 2018 experiments the hole at the base of the test cell was partially sealed and the media was replanted, see Text S9, SI), the different study designs (alternating bromide-free and bromide-spiked storms in 2018 versus a single bromide-spiked storm followed by multiple bromide-free storms in 2019), or differences in how the model was calibrated (minimizing the RMSE based on outflow concentrations from a single bromide-spiked storm in 2018 versus outflow concentrations from four bromide-free storms following the bromide-spiked storm in 2019).

Implications for Age Structure and Pollutant Removal

5.1 Age Distribution of Water Leaving the Biofilter by Gravitational Discharge

What can TTD theory tell us about the age structure of water leaving the biofilter by gravitational discharge? By selecting a uniform rSAS function for our model (Section 2.3.2), the backward TTDs for gravitational discharge and ET are equal to the RTD of water stored in the biofilter. Thus, under uniform storage sampling, the age distribution of water in storage is equal to the age distribution of water leaving the biofilter as gravitational discharge.

During the 2018 experiments, predictions for the median age of water stored in the biofilter (equation (7a) and discussion thereof) follows a semi-periodic pattern, increasing linearly with time between storms (as water stored in the biofilter ages) and rapidly declining to near zero during storm events (as incoming stormwater, of age $T=0$ h, fills the biofilter, Figure 5a). The 5th and 50th (median) age percentiles overlap but the 95th age percentile is much older, indicating that the age distribution is positively skewed (Ang & Tang, 2007). The 5th and 50th percentiles overlap because, at any time t, more than 50% of water stored in the biofilter is from the most recent storm with an age roughly equal to the antecedent dry period. The 95th percentile age is much older because the rest of water in storage (i.e., water not from the last storm) is from penultimate and earlier storms.

For the simulations presented in Figure 5a we arbitrarily set the initial age of "original" water (i.e., water that was initially present in the biofilter at time, $t=0$) at $T_0 =$ 50 h. Until the fourth storm, this original water constituted more than 5% of water stored in the biofilter, as evidenced by the upward slope of the grey band in Figure 5a (the upward slope reflects the fact that that original water in storage is aging linearly with time). After the fourth storm, the original water's contribution to storage drops below 5%, as evidenced by a steep drop in the 95th percentile around $t = 28$ h (Figure 5a). Thus, four storms were required to flush out 95% of the original water, even though more than 50% of water in the biofilter, at any given time, is from the last storm. A similar pattern is evident for the set of experiments conducted in 2019 (Figure 5b). Across both years the mean age is 5 to 20 hours older than the median age, consistent with a positively skewed age distribution (Ang & Tang, 2007).

5.2 Mapping out the Contribution of Past Storms to Present Storage

TTD theory also allows us to determine the relative contribution of all past storms to water stored in a biofilter at any time, t. If the n-th storm begins at time, $t = t_{b,n}$, then the fraction, $f_n(t)$ [-], of water in storage with that age or younger can be estimated from the RTD's CDF (see Section 2.3.4) (Kirchner, 2016; Benettin et al., 2017; Lutz et al., 2018):

$$f_n(t) = P_{\mathrm{RTD}}^{U}\left(T = t - t_{b,n}, t\right),\ t > t_{b,n} \tag{10}$$

We applied equation (10) to all seven storms simulated in 2019, along with the original water present in the biofilter at time, $t = 0$ (Figure 6). The upper bound of each color band represents the fraction of water in storage that is younger than the oldest water from the storm indicated. The lower bound of the same color band represents the fraction of water in storage that is younger than the oldest water from the next storm, and so on.

The influence of biofilter hydrology on the age structure of stored water (and by implication the age structure of water leaving the biofilter by gravitational drainage under uniform sampling) is striking. During the Filling Phase of each storm (e.g., Storm #3 in Figure 6) new water entering the biofilter from the ponding zone rapidly dominates the age distribution of water in storage for two reasons: (1) the new water fills up portions of

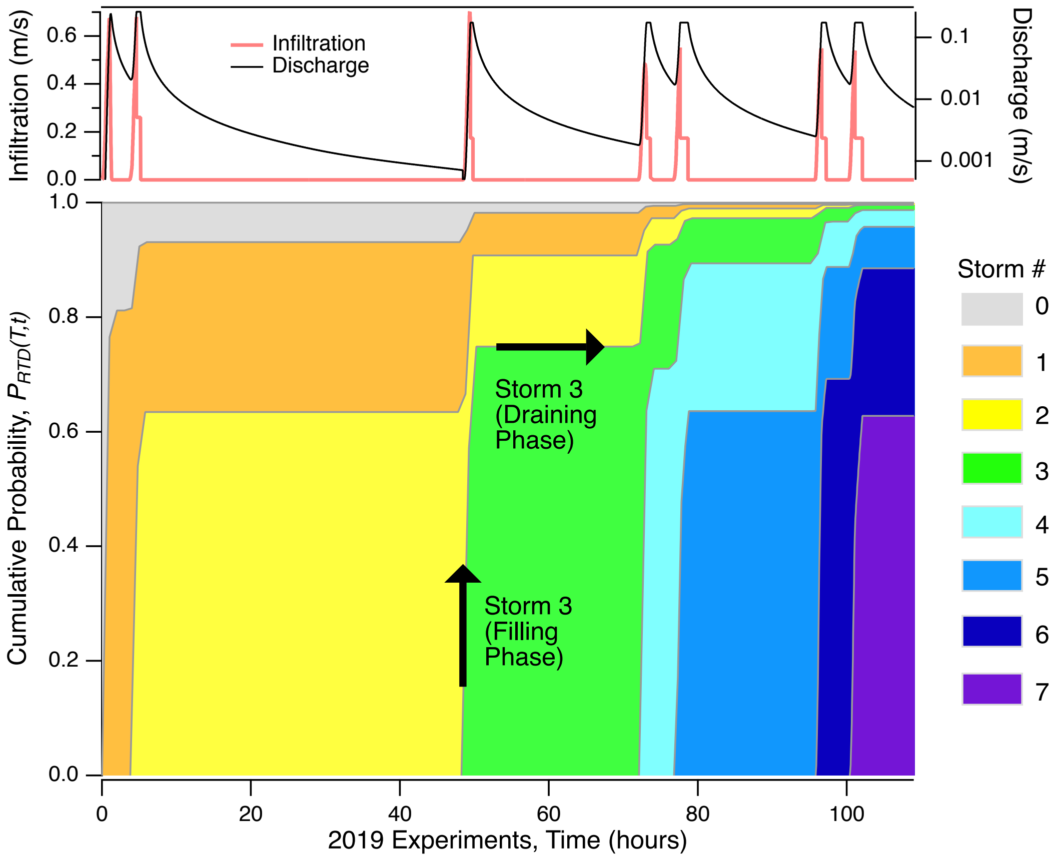

Figure 6. The contribution of original water (Storm #0) and seven experimental storms in 2019 (Storms #1-7) to water storage in the OCPW biofilter over time. Each new storm rapidly occupies at least 50% of storage volume during the Filling Phase. These simulations were carried out using the inferred value for maximum storage of S_{max} = 0.42 m. Top panel indicates infiltration (red curve) and discharge (black curve) for the 2019 storm sequence.

storage that were previously dry; and (2) the new water displaces older water, driving it out of the biofilter as gravitational drainage. The first mechanism explains why different storms initially dominate storage to different degrees. For example, the volume of original water in storage at time $t=0$ was relatively small in these simulations ($S_0=0.092$ m, corresponding to the biofilter's field capacity) which explains why Storm #1 very quickly constituted more than 80% of the biofilter's storage (orange band in Figure 6). Under a uniform rSAS, all water parcels (regardless of their age) have an equal probability of being selected for outflow by gravitational discharge or ET. This explains why, during the

Draining Phase, the age structure of water in storage does not change (i.e., during this phase all boundaries in Figure 6 are horizontal lines). Figure 6 also vividly illustrates the two key attributes of biofilter storage discussed previously: at any time about >50% of water in storage is from the most recent storm while the rest is a mixture of penultimate and earlier storms.

5.3 Age Structure and Water Quality

The age structure of water in storage has significant implications for the treatment credit attributable to, and the pollution exported by, GSI. For example, during the 2019 storm sequence we included a "worst case" scenario (from a water quality perspective) by using a 50:50 mixture of stormwater and raw sewage for one of the storm events, Storm #3. What does TTD theory tell us about how long sewage from Storm #3 lingers in the biofilter during subsequent flushing events? From the thickness of the green band in Figure 6 we can infer that the percent of storage attributable to raw sewage during the drainage phase of each storm declined over time as follows: 35% (Storm #3), 11% (Storm #4), 4% (Storm #5), 1.2% (Storm #6), and 0.5% (Storm #7). Raw sewage harbors very high concentrations of human fecal bacteria (e.g., in the range of 10^6 *E. coli* mL^{-1} (Garcia-Aljaro et al., 2018)). Therefore, even after the biofilter has been flushed with four sewage-free storms, the *E. coli* concentration in gravitational drainage could still be as high as 5000 mL^{-1}—more than enough bacteria to close beaches if the biofilter drained to a recreational lake or river (US EPA, 2018)). This example assumes that bacteria behave conservatively which is rarely the case (Lee et al., 2006; Chandrasena et al., 2014b).

Indeed, the retention of older water in the biofilter could impact the quality of water leaving a biofilter by gravitational drainage either positively or negatively, depending on inter-storm pollutant transformation mechanisms. For example, between storms the biofilter media's organic material can be respired by resident bacteria, potentially leading to the liberation of ammonium (by ammonification) and nitrate (by nitrification) (Canfield et al., 2010). Thus, water retained in the biofilter from penultimate and older storms could serve as a perpetual source of nitrate that is exported during storm events—a pattern often observed in practice (e.g., Hatt et al., 2009; McPhillips et al., 2018). On the other hand, if anaerobic conditions develop between storms (as is likely to occur if the biofilter contains a submerged zone (Kim et al., 2003)) nitrate may be further transformed to harmless N_2 gas and, potentially, the potent greenhouse gas N_2O (McPhillips et al., 2018) by denitrification. Studies are underway to extend the TTD results presented here to include the fate and transport of human pathogens, microbial communities, nutrients, and heavy metals during and the 2019 storm sequence.

6. Conclusions

TTD theory directly links the hydrology and treatment performance of GSI. Its practical application therefore requires, as a first step, delineation of the unsteady water balance over the GSI element of interest. In this paper we demonstrate that this first step can be accomplished with a simple bucket model that tracks time varying infiltration, storage, ET and gravitational discharge over a control volume drawn around the biofilter media, which in our case was lined with an underdrain open to the atmosphere. To operationalize the water balance bucket model, a parsimonious set of expressions were developed and tested for the storage-dependence of water moving in and out of the control volume, including: (1) an empirical relationship for infiltration that toggles between the inflow rate of stormwater (when the biofilter media is partially unsaturated) and the saturated hydraulic conductivity (when the biofilter media approaches full saturation); (2) cPET for ET; and (3) Kirchner's power-law model for gravitational discharge (Kirchner, 2009).

Generalizing the water balance bucket model beyond the experimental system described here may require modifying (1) and (2), for example by adopting a process-based model (such as the Green-Ampt equation (Green & Ampt, 1911)) for infiltration and accounting for the reduction of ET that occurs when saturation falls below the incipient water stress (Hess et al., 2019; Zhao et al., 2013). On the other hand, three lines of evidence suggest that Kirchner's model for gravitational drainage may be more generally applicable. First, the power-law model's two empirical parameters (S_{min} and g) appear robust to antecedent dry period and changes in saturated hydraulic conductivity. Second, values inferred for these two parameters are concordant with what we know about our biofilter, namely that it does not have a submerged zone ($S_{min}=0$) and, compared to a catchment, has relatively little storage volume ($g=5$ translates to a recessional exponent of $b=1.8$, indicating that drainage from the biofilter is flashy). Indeed, we hypothesize that, in general, S_{min} can be equated to the area-normalized volume of the submerged zone (Kim et al., 2003; Brown & Hunt, 2011). Finally, our inferred exponent value ($g=5$) is consistent with a previously published estimate for the power-law dependence of gravitational drainage on storage in the vadose zone of a 46 km^2 catchment (Bertuzzo et al., 2013) (the area-normalized volume of this catchment's vadose zone is similar to the area-normalized volume of our biofilter, *ca*. 0.1 to 0.2 m). That leaves the area normalized volume (S_{max}) of the biofilter, which may exceed the biofilter's physical void volume due to exfiltration.

With the unsteady water balance in hand, we next solved the age conservation equation under the assumption that stored water is randomly selected for outflow regardless of its age (i.e., we adopted the uniform rSAS function). From this solution explicit expressions were derived for the mean age of water in storage (and leaving the biofilter as ET and gravitational discharge), various age percentiles, as well as the breakthrough concentration of a solute with or without first-order reaction (equations (8c) and (9b)). When compared to bromide breakthrough measured during our field experiments, we find the model over samples young water, either because the uniform rSAS function oversamples young water in storage, or because there is simply not enough old water in storage to sample from (Benettin et al., 2013; Harman, 2015).

Given the magnitude of lateral exfiltration in our system, it is unlikely that water entering the outflow tank was selected exclusively from water stored within the physical boundaries of the biofilter test cell. Indeed, when we allow the volume of the biofilter to be a free variable, the inferred volumes are 70% to 196% larger than the the biofilter's void volume, consistent with the hypothesis that exfiltration increases the effective storage experienced by solutes as they transit through the system. The concordance between predicted and measured bromide breakthrough concentrations improves dramatically after taking this extra storage into account (Figures 4b and 4d). Remarkably, the final model—which includes both the unsteady water balance over the biofilter media (equation (1a)) and the convolution integral for solute breakthrough (equation (9b))—has only one fitting parameter: the effective volume of the biofilter, $S_{\max}$. The parsimony and predictive power of TTD theory make it ideally suited to model pollutant removal at the scale of individual biofilters, as well as GSI networks and the urban catchments in which they are embedded.

Acknowledgments

The authors declare no conflict of interest. All data used in this study are publicly available (http://www.hydroshare.org/resource/b7187928719446bbaf30d181787efdad). Funding was provided by the University of California Office of the President, Multicampus Research Programs and Initiatives, Grant ID MRP-17-455083, Virginia Tech's Charles E. Via, Jr. Department of Civil and Environmental Engineering, and U.S. National Science Foundation (award 1840504). EAP was supported by a Via Ph.D. Fellowship from Virginia Tech's Charles E. Via, Jr. Department of Civil and Environmental Engineering. The authors thank E. Fassman-Beck, B. Hong, A. Mehring, and OCPW staff, for their assistance with field sampling and lab analysis. EAP and SBG designed and implemented the experiments, derived the TTD framework, and drafted the manuscript. YC, JP, SS coordinated field experiments. MAR, PH, MF, SA, HL, WH, MR, JJ, DL contributed to field sampling and lab analysis. MAR, SS, and KM contributed analyses. All co-authors contributed edits.

References

Alikhani, J., Nietch, C., Jacobs, S., Shuster, B., & Massoudieh, A. (2020). Modeling and design scenario analysis of long-term monitored bioretention system for rainfall-runoff reduction to combined sewer in Cincinnati, OH. *Journal of Sustainable Water in the Built Environment, 6*(2), 04019016.

Allen, R. G., Pereira, L. S., Raes, D., & Smith, M. (1998). Crop evapotranspiration – Guidelines for computing crop water requirements – FAO Irrigation and Drainage Paper 56. Food and Agriculture Organization of the United Nations.

Al-Mashaqbeh, O., & McLaughlan, R. G. (2012) Non-equilibrium zinc uptake onto compost particles from synthetic stormwater. *Bioresource Technology, 123*, 242-248.

Ambrose, R. F., & Winfrey, B. K. (2015). Comparison of stormwater biofiltration systems in Southeast Australia and Southern California. *WIREs Water, 2,* 131-146.

Ang, A. H-S., & Tang, W. H. (2007) *Probability Concepts in Engineering: Emphasis on Applications to Civil and Environmental Engineering,* 2nd edition. Hoboken, NJ: John Wiley & Sons, Inc.

Bedan, E. S., & Clausen, J. C. (2009). Stormwater Runoff Quality and Quantity from Traditional and Low Impact Development Watersheds. *Journal of the American Water Resources Association, 45*(4), 998-1008.

Behroozi, A., Arora, M., Fletcher, T. D., & Western, A. W. (2020). Sorption and transport behavior of zinc in the soil; Implications for stormwater management. *Geoderma, 367,* 114243.

BenDor, T. K., Shandas, V., Miles, B., Belt, K., & Olander, L. (2018). Ecosystem services and U.S. stormwater planning: An approach for improving urban stormwater decisions. *Environmental Science & Policy*, *88*, 92-103.

Benettin, P., Rinaldo, A., Botter, G. (2013) Kinematics of age mixing in advection-dispersion models. *Water Resources Research 49*, 8539-8551. doi:10.1002/2013WR014708

Benettin, P., Bailey, S. W., Campbell, J. L., Green, M. B., Rinaldo, A., Likens, G. E., McGuire, K. J., & Botter, G. (2015b). Linking water age and solute dynamics in streamflow at the Hubbard Brook Experimental Forest, NH, USA, *Water Resources Research, 51,* 9256–9272, doi:10.1002/2015WR017552.

Benettin, P., Rinaldo, A., & Botter, G. (2015a). Tracking residence times in hydrological systems: Forward and backward formulations. *Hydrological Processes*, *29*(25), 5203-5213.

Benettin, P., Bailey, S. W., Rinaldo, A., Likens, G. E., McGuire, K. J., & Botter, G. (2017). Young runoff fractions control streamwater age and solute concentration dynamics. *Hydrological Processes*, *31*(16), 2982-2986.

Bertuzzo, E., Thomet, M., Botter, G., & Rinaldo, A. (2013). Catchment-scale herbicides transport: Theory and application. *Advances in Water Resources, 52,* 232-242.

Boehm, A. B., Bell, C. D., Fitzgerald, N. J. M., Gallo, E., Higgins, C. P., Hogue, T. S., et al. (2020). Biochar-augmented biofilters to improve pollutant removal from stormwater – can they improve receiving water quality? *Environmental Science: Water Research & Technology, 6,* 1520-1537.

Boivin, A., Simunek, J., Schiavon, M., & van Genuchten, M. (2006). Comparison of Pesticide Transport Processes in Three Tile-Drained Field Soils Using HYDRUS-2D. *Vadose Zone Journal, 5*(3), 838-849.

Botter, G., Bertuzzo, E., & Rinaldo, A. (2011). Catchment residence and travel time distributions: The master equation. *Geophysical Research Letters, 38*(11), L11403. doi:10.1029/2011GL047666

Brooks, K. N., Ffolliott, P. F., & Magner, J. A. (2013). *Hydrology and the Management of Watersheds* (4th Edition). Ames, IA: John Wiley & Sons, Inc.

Brown, R. A., & Hunt, W. F. (2011). Underdrain configuration to enhance bioretention exfiltration to reduce pollutant loads. *Journal of Environmental Engineering, 137*(11), 1082-1091. https://doi.org/10.1061/(ASCE)EE.1943-7870.0000437

Browne, D., Deletic, A., Mudd, G. M., & Fletcher, T. D. (2008). A new saturated/unsaturated model for stormwater infiltration systems. *Hydrological Processes, 22,* 4838-4849.

Canfield, D.E., Glazer, A.N., & Falkowski, P.G. (2010) The evolution and future of Earth's nitrogen cycle. *Science, 330*, 192-196.

Chandrasena, G. I., Deletic, A., & McCarthy, D. T. (2014b). Survival of Escherichia coli in stormwater biofilters. *Environmental Science and Pollution Research, 21*(8), 5391-5401.

Chandrasena, G. I., Pham, T., Payne, E. G. I., Deletic, A., & McCarthy, D. T. (2014a). E. coli removal in laboratory scale stormwater biofilters: Influence of vegetation and submerged zone. *Journal of Hydrology*, *519*, 814-822.

Clar, M. L., Barfield, B. J., & O'Connor, T.P. (2004). Stormwater Best Mangement Practice Design Guide Volume 2: Vegetative Biofilters, EPA/600/R-04/121A, Washington, DC: U.S. Environmental Protection Agency.

Daly, E., Deletic, A., Hatt, B. E., & Fletcher, T. D. (2012). Modelling of stormwater biofilters under random hydrologic variability: a case study of a car park at Monash University, Victoria (Australia). *Hydrological Processes*, *26*, 3416-3424.

Danesh‐Yazdi, M., Klaus, J., Condon, L. E., & Maxwell, R. M. (2018). Bridging the gap between numerical solutions of travel time distributions and analytical storage selection functions. *Hydrological Processes*, *32*(8), 1063-1076.

Davis, J.C. (2002), "Statistics and Data Analysis in Geology, 3rd Ed." John Wiley & Sons, Inc. New York, 638pp.

Davis, A. P. (2008). Field performance of bioretention: hydrology impacts. *Journal of Hydrologic Engineering, 13*(2), 90-95. DOI: 10.1061/(ASCE)1084-0699(2008)13:2(90)

Davis, A. P., Hunt, W. F., Traver, R. G., & Clar, M. (2009). Bioretention Technology: Overview of Current Practice and Future Needs. *Journal of Environmental Engineering, 135*(3), 109-117.

Dos Santos, D. R., Cambier, P., Mallmann, F. J. K., Labanowski, J., Lamy, I., Tessier, D., & van Oort, F. (2013). Prospective modeling with Hydrus-2D of 50 years Zn and Pb movements in low and moderately metal-contaminated agricultural soils. *Journal of Contaminant Hydrology, 145,* 54-66.

Engemann, K., Pedersen, C. B., Arge, L., Tsirogiannis, C., Mortensen, P. B., & Svenning, J. C. (2019). Residential green space in childhood is associated with lower risk of psychiatric disorders from adolescence into adulthood. *Proceedings of the National Academy of Sciences*, *116*(11), 5188-5193.

eWater Ltd. (2020) Model for Urban Stormwater Improvement Conceptualization MUSICX. Bruce, ACT, Australia.

Feng, W., Hatt, B. E., McCarthy, D. T., Fletcher, T. D., & Deletic, A. (2012). Biofilters for Stormwater Harvesting: Understanding the Treatment Performance of Key Metals That Pose a Risk for Water Use. *Environmental Science & Technology*, *46*(9), 5100-5108.

Garcia-Aljaro, C., Blanch, A. R., Campos, C., Jofre, J., & Lucena, F. (2018). Pathogens, faecal indicators and human specific microbial source-tracking markers in sewage. *Journal of Applied Microbiology, 126,* 701-717.

Grant, S. B., Fletcher, T. D., Feldman, D., Saphores, J. D., Cook, P. L. M., Stewardson, M., et al. (2013). Adapting Urban Water Systems to a Changing Climate: Lessons from the Millennium Drought in Southeast Australia. *Environmental Science & Technology, 47*(19), 10727-10734.

Grebel, J. E., Mohanty, S. K., Torkelson, A. A., Boehm, A. B., Higgins, C. P., Maxwell, R. M., et al. (2013). Engineered Infiltration Systems for Urban Stormwater Reclamation. *Environmental Engineering Science*, *30*(8), 437–454.

Green, W. H., & Ampt, G. A. (1911). Studies on Soil Physics, Part 1, The Flow of Air and Water through Soils. *Journal of Agricultural Science, 4*, 11-24.

Harman, C. J. (2015). Time-variable transit time distributions and transport: Theory and application to storage-dependent transport of chloride in a watershed. *Water Resources Research, 51,* 1-30. doi:10.1002/2014WR015707

Harman, C. J. (2019). Age-Ranked Storage-Discharge Relations: A Unified Description of Spatially Lumped Flow and Water Age in Hydrologic Systems. *Water Resources Research, 55*(8), 7143-7165. doi:10.1029/2017WR022304

Hatt, B. E., Fletcher, T. D., & Deletic, A. (2009). Hydrologic and pollutant removal performance of stormwater biofiltration systems at the field scale. *Journal of Hydrology*, *365*(3-4), 310-321.

Henrichs, M., Welker, A., & Uhl, M. (2009). Modelling of biofilters for ammonium reduction in combined sewer overflow. *Water Science & Technology, 60*(3), 825-831.

Hess, A., Wadzuk, B., & Welker, A. (2019). Predictive Evapotranspiration Equations in Rain Gardens. *Journal of Irrigation and Drainage Engineering, 145*(7), 04019010.

Horel, A., Schiewer, S., & Misra, D. (2015). Effect of concentration gradients on biodegradation in bench-scale sand columns with HYDRUS modeling of hydrocarbon transport and degradation. *Environmental Science and Pollution Research, 22,* 13251-13262.

Hrachowitz, M., Benettin, P., van Breukelen, B. M., Fovet, O., Howden, N. J. K., Ruiz, L., et al. (2016). Transit times – the link between hydrology and water quality at the catchment scale. *WIREs Water*, *3*, 629-657.

Jefferson, A. J., Bhaskar, A. S., Hopkins, K. G., Fanelli, R., Avellaneda, P. M., & McMillan, S. K. (2017). Stormwater management network effectiveness and implications for urban watershed function: A critical review. *Hydrological Processes, 31*(23), 4056-4080.

Jiang, C., Li, J., Li, H., & Li, Y. (2019). Experiment and simulation of layered bioretention system for hydrological performance. *Journal of Water Reuse and Desalination, 9*(3), 319-329.

Jiang, S., Pang, L., Buchan, G. D., Simunek, J., Noonan, M. J., & Close, M. E. (2010). Modeling water flow and bacterial transport in undisturbed lysimeters under irrigations of dairy shed effluent and water using HYDRUS-1D. *Water Research, 44*(4), 1050-1061.

Keeler, B. L., Hamel, P., McPhearson, T., Hamann, M. H., Donahue, M. L., Meza Prado, K. A., et al. (2019). Socio-ecological and technological factors moderate the value of urban nature. *Nature Sustainability*, *2*, 29-38.

Kim, H., Seagren, E.A., & Davis, A.P (2003), Engineered bioretention for removal of nitrate from stormwater runoff, *Water Environment Research 75*(4), 355-367.

Kim, M., Pangle, L. A., Cardoso, C., Lora, M., Volkmann, T. H. M., Wang, Y., Harman, C. J., & Troch, P. A. (2016). Transit time distributions and StorAge Selection functions in a sloping soil lysimeter with time-varying flow paths: Direct observation of internal and external transport variability, *Water Resources Research, 52*, 7105–7129, doi:10.1002/2016WR018620.

Kirchner, J. W. (2009). Catchments as simple dynamical systems: Catchment characterization, rainfall-runoff modeling, and doing hydrology backward. *Water Resources Research, 45,* W02429. doi:10.1029/2008WR006912

Kirchner, J. W. (2016). Aggregation in environmental systems-Part 1: Seasonal tracer cycles quantify young water fractions, but not mean transit times, in spatially heterogeneous catchments. *Hydrology and Earth System Sciences*, *20*(1), 279-297.

Kranner, B. P., Afrooz, A. R. M. N., Fitzgerald, N. J. M., & Boehm, A. B. (2019). Fecal indicator bacteria and virus removal in stormwater biofilters: Effects of biochar, media saturation, and field conditioning. *PLoS One*, *14*(9), e0222719.

Le Coustumer, S., Fletcher, T. D., Deletic, A., Barraud, S., & Lewis, J. F. (2009). Hydraulic performance of biofilter systems for stormwater management: Influences of design and operation. *Journal of Hydrology, 376*(1-2), 16-23.

Le Coustumer, S., Fletcher, T. D., Deletic, A., Barraud, S., & Poelsma, P. (2012). The influence of design parameters on clogging of stormwater biofilters: A large-scale column study. *Water Research, 46*(20), 6743-6752.

Lee, J. G., Borst, M., Brown, R. A., Rossman, L., Simon, M. A. (2015). Modeling the hydrologic processes of a permeable pavement system. *Journal of Hydrologic Engineering, 20*(5), 1-9.

Lee, C. M., Lin, T. Y., Lin, C., Kohbodi, G. A., Bhatt, A., Lee, R., Jay, J. A. (2006). Persistence of fecal indicator bacteria in Santa Monica Bay beach sediments. *Water Research, 40*(14), 2593-2602.

LeFevre, G. H., Paus, K. H., Natarajan, P., Gulliver, J. S., Novak, P. J., & Hozalski, R. M. (2015). Review of Dissolved Pollutants in Urban Storm Water and Their Removal and Fate in Bioretention Cells. *Journal of Environmental Engineering, 141*(1), 04014050.

Li, C., Fletcher, T. D., Duncan, H. P., & Burns, M. J. (2017). Can stormwater control measures restore altered urban flow regimes at the catchment scale? *Journal of Hydrology 549,* 631-653.

Li, L., & Davis, A. P. (2014). Urban Stormwater Runoff Nitrogen Composition and Fate in Bioretention Systems. *Environmental Science & Technology*, 48(6), 3403-3410.

Li, Y., Deletic, A., Alcazar, L., Bratieres, K., Fletcher, T. D., & McCarthy, D. T. (2012). Removal of Clostridium perfringens, Escherichia coli and F-RNA coliphages by stormwater biofilters. *Ecological Engineering*, *49*, 137-145.

Li, Y., McCarthy, D. T., & Deletic, A. (2016). *Escherichia coli* removal in copper-zeolite-integrated stormwater biofilters: Effect of vegetation, operational time, intermittent drying weather. *Ecological Engineering*, *90*, 234-243.

Lutz, S. R., Krieg, R., Müller, C., Zink, M., Knöller, K., Samaniego, L., & Merz, R. (2018). Spatial patterns of water age: Using young water fractions to improve the characterization of transit times in contrasting catchments. *Water Resources Research*, *54*(7), 4767-4784. https://doi.org/10.1029/2017WR022216

Massoudieh, A., Maghrebi, M., Kamrani, B., Nietch, C., Tryby, M., Aflaki, S., & Panguluri, S. (2017). A flexible modeling framework for hydraulic and water quality performance assessment of stormwater green infrastructure. *Environmental Modelling & Software, 92,* 57-73.

McPhillips, L, Goodale, C., Walter, T. (2018) Nutrient leaching and greenhouse gas emissions in grassed detention and bioretention stormwater basins. *Journal of Sustainable Water in the Built Environment, 4*(1), doi: 10.1061/JSWBAY.0000837.

Metzler, H., Muller, M., & Sierra, C. A. (2018). Transit-time and age distributions for nonlinear time-dependent compartmental systems. *Proceedings of the National Academy of Sciences, 115*(6), 1150-1155.

Mohanty, S. K., & Boehm, A.B. (2014). *Escherichia coli* Removal in Biochar-Augmented Biofilter: Effect of Infiltration Rate, Initial Bacterial Concentration, Biochar Particle Size, and Presence of Compost. *Environmental Science & Technology*, *48*(19) 11535-11542.

National Academies of Sciences, Engineering, and Medicine. (2016). *Using Graywater and Stormwater to Enhance Local Water Supplies: An Assessment of Risks, Costs, and Benefits.* Washington, DC: The National Academies Press.

Niemi, A. J. (1977). Residence Time Distributions of Variable Flow Processes. *International Journal of Applied Radiation and Isotopes, 28,* 855-860.

Orange County Public Works (2017). Prop. 84 OC Public Works Glassell Campus Stormwater LID Retrofit Project Final Report PIN 24108. Orange, CA.

Payne, E. G. I., Hatt, B. E., Deletic, A., Dobbie, M. F., McCarthy, D. T., & Chandrasena, G. I. (2015). Adoption Guidelines for Stormwater Biofiltration Systems - Summary Report. Melbourne, Australia: Cooperative Research Centre for Water Sensitive Cities.

Payne, E. G. I., Pham, T., Cook, P. L. M., Fletcher, T. D., Hatt, B. E., & Deletic, A. (2014). Biofilter design for effective nitrogen removal from stormwater – influence of plant species, inflow hydrology and use of a saturated zone. *Water Science & Technology, 69*(6), 1312-1319.

Payne, E. G. I., Pham, T., Deletic, A., Hatt, B. E., Cook, P. L. M., & Fletcher, T. D. (2018). Which species? A decision-support tool to guide plant selection in stormwater biofilters. *Advances in Water Resources*, *113*, 86-99.

Peng, J., Cao, Y., Rippy, M. A., Afrooz, A. R. M. N., Grant, S. B. (2016). Indicator and Pathogen Removal by Low Impact Development Best Management Practices. *Water 8*(12), 600.

Radcliffe, D., & Simunek, J. (2010). *Soil Physics with HYDRUS.* Boca Raton, FL: CRC Press.

Randelovic, A., Zhang, K., Jacimovic, N., McCarthy, D., & Deletic, A. (2016). Stormwater biofilter treatment model (MPiRe) for selected micro-pollutants. *Water Research, 89,* 180-191.

Raymond, C. M., Frantzeskaki, N., Kabisch, N., Berry, P., Breil, M., Nita, M. R., et al. (2017). A framework for assessing and implementing the co-benefits of nature-based solutions in urban areas. *Environmental Science & Policy*, *77*, 15-24.

Read, J., Wevill, T., Fletcher, T., & Deletic, A. (2008). Variation among plant species in pollutant removal from stormwater in biofiltration systems. *Water Research*, *42*(4-5), 893-902.

Read, J., Fletcher, T. D., Wevill, T., Deletic, A. (2009). Plant Traits that Enhance Pollutant Removal from Stormwater in Biofiltration Systems. *International Journal of Phytoremediation*, *12*(1), 34-53.

Rinaldo, A., Benettin, P., Harman, C. J., Hrachowitz, M., McGuire, K. J., Van Der Velde, Y., Bertuzzo, E., & Botter, G. (2015). Storage selection functions: A coherent framework for quantifying how catchments store and release water and solutes. *Water Resources Research*, *51*(6), 4840-4847. https://doi.org/10.1002/2015WR017273

Rinaldo, A., Beven, K. J., Bertuzzo, E., Nicotina, L., Davies, J., Fiori, A., Russo, D., & Botter, G. (2011). Catchment travel time distributions and water flow in soils. *Water Resources Research*, *47*, W07537. https://doi.org/10.1029/2011WR010478

Rippy, M. A. (2015). Meeting the criteria: linking biofilter design to fecal indicator bacteria removal. *Wiley Interdisciplinary Reviews: Water, 2*(5), 577-592.

Rodriguez, N. B., McGuire, K. J., & Klaus, J. (2018). Time-varying storage– Water age relationships in a catchment with a Mediterranean climate. *Water Resources Research, 54*, 3988–4008. https://doi.org/10.1029/ 2017WR021964

Roy-Poirier, A., Champagne, P., & Filion, Y. (2010). Review of Bioretention System Research and Design: Past, Present, and Future. *Journal of Environmental Engineering 136*(9), 878-889.

Rycewicz-Borecki, M., McLean, J. E., & Dupont, R. R. (2017). Nitrogen and phosphorous mass balance, retention and uptake in six plant species grown in stormwater bioretention microcosms. *Ecological Engineering*, *99*, 409-416.

Shen, P., Deletic, A., Urich, C., Chandrasena, G. I., & McCarthy, D. T. (2018). Stormwater biofilter treatment model for faecal microorganisms. *Science of the Total Environment 630,* 992-1002.

Simunek, J., van Genuchten, M., & Sejna, M. (2008). Development and Applications of the HYDRUS and STANMOD Software Packages and Related Codes. *Vadose Zone Journal, 7*(2), 587-600.

Smith, A. A., Tetzlaff, D., & Soulsby, C. (2018). On the Use of StorAge Selection Functions to Assess Time-Variant Travel Times in Lakes. *Water Resources Research, 54,* 5163-5185. https://doi.org/10.1029/2017WR021242

Trenouth, W. R., & Gharabaghi, B. (2015). Soil amendments for heavy metals removal from stormwater runoff discharging to environmentally sensitive areas. *Journal of Hydrology, 529*(3), 1478-1487.

Ulrich, B. A., Vignola, M., Edgehouse, K., Werner, D., & Higgins, C. P. (2017). Organic Carbon Amendments for Enhanced Biological Attenuation of Trace Organic Contaminants in Biochar-Amended Stormwater Biofilters. *Environmental Science & Technology, 51*(16), 9184-9193.

U. S. Environmental Protection Agency. (2018). 2017 Five-Year Review of the 2012 Recreational Water Quality Criteria. EPA-823-R-18-001. Washington, DC: Office of Water, US EPA.

Walsh, C. J., Booth, D. B., Burns, M. J., Fletcher, T. D., Hale, R. L., Hoang, L. N., et al. (2016). Principles for urban stormwater management to protect stream ecosystems. *Freshwater Science, 35*(1), 398-411.

Walsh, C.J., Fletcher, T.D., & Burns, M.J. (2012). Urban stormwater runoff: A new class of environmental flow problem. *PLoS One*, *7*, e45814.

Walsh, C. J., Roy, A. H., Feminella, J. W., Cottingham, P. D., Groffman, P. M., & Morgan, R. P. (2005). The urban stream syndrome: current knowledge and the search for a cure. *Journal of the North American Benthological Society*, *24*, 706–723.

Williams, J. R., Ouyang, Y., Chen, J., & Ravi, V. (1998). Estimation of Infiltration Rate in Vadose Zone: Application of Selected Mathematical Models Volume II. EPA/600/R-97/128b, Ada, OK: National Risk Management Research Laboratory, U.S. Environmental Protection Agency.

Winston, R. J., Dorsey, J. D., & Hunt, W. F. (2016). Quantifying volume reduction and peak flow mitigation for three bioretention cells in clay soils in northeast Ohio. *Science of the Total Environment, 553,* 83-95.

Wong, T. H. F. (2006). Water sensitive urban design – the journey thus far. *Australasian Journal of Water Resources, 10* (3), 213-222.

Zhang, K., Randelovic, A., Deletic, A., Page, D., & McCarthy, D. T. (2019). Can we use a simple modeling tool to validate stormwater biofilters for herbicides treatment? *Urban Water Journal, 16*(6), 412-420.

Zhang, L., Seagren, E. A., Davis, A. P., & Karns, J. S. (2010). The Capture and Destruction of *Escherichia coli* from Simulated Urban Runoff Using Conventional Bioretention Media and Iron Oxide-coated Sand. *Water Environment Research*, *82*(8), 701-714.

Zhao, L., Xia, J., Xu, C., Wang, Z., Sobkowiak, L., & Long, C. (2013). Evapotranspiration estimation methods in hydrological models. *Journal of Geographical Sciences, 23*(2), 359-369.